Chapter 1
Physical Properties of Unconventional Superconductors

The introduction part of the book is devoted to the description of physical properties of advanced classes of superconductors: cuprate superconductors, borocarbides, magnesium diboride, and oxypnictides. Description of crystal structure, electronic properties, and related theoretical models for each group of superconductors is presented. Anisotropy and multiband effects are specially emphasized. Well-known and generally accepted results of computed Fermi surface of these compounds and Fermi liquid properties are included to first part. Results of order parameter symmetry, its relation with possible pairing mechanism, and general consequences for experimentally accessible properties investigations in this class of superconductors are presented. Different vortex states in advanced classes of superconductors and experimental results of related phenomena are also considered. The rich variety of superconducting compounds in the advanced class of superconductors and the growing knowledge of their electronic structure can be helpful to clarify differences and similarities with other exotic superconductors.

1.1 Cuprate Superconductors

In more than 24 years elapsed from the discovery of high T_c superconductivity in cooper oxides [1], a huge number of experimental and theoretical investigations of the physical properties of these materials have been done. The high-temperature superconductivity of cuprates was discovered in 1986 [1], when the highest superconducting transition temperature (i.e., critical temperature) characteristic of conventional superconductors ($T_c = 23.2$ K in Nb_3 Ge) was substantially exceeded and a superconducting transition temperature $T_c = 30$ K was achieved in the ceramic $La_{2-x}Ba_xCuO_{4-\delta}$. Within a year after this discovery, the record value of T_c exceeded 90 K ($YBa_2Cu_3O_{7-\delta}$ ceramic). The further search for and creation of new superconducting materials led to $T_c = 138$ K (Tl-doped $HgBa_2Ca_2Cu_3O_{8-\delta}$ compound) in 1994 and raised the question of room-temperature superconductivity. In spite of all these efforts, the mechanism of this new kind of superconductivity

I. Askerzade, *Unconventional Superconductors*, Springer Series in Materials Science 153,
DOI 10.1007/978-3-642-22652-6_1, © Springer-Verlag Berlin Heidelberg 2012

has not been clarified yet; it still remains one of the most enigmatic problems of the solid-state physics [2–4]. The description of their normal state properties [5, 6] has turned out to represent an even bigger challenge to solid-state physics theory. The difficulty of this problem is due to the complicated properties, including complicated crystalline structures of materials displaying high T_c, to the presence of a strong anisotropy, to the existence of non-adiabatic effects, to strong electronic correlations, and to a strong electron–phonon interaction.

In these complicated materials, several phase transitions (structural, magnetic, superconductor, etc.) occur, and mixed states are allowed, for instance coexistence of superconductivity and ferromagnetism or vitreous spin state. The key structural element of layered quasi-two-dimensional cuprates is a (CuO_2) plane (one or several in a unit cell); they differ from conventional superconductors not only in high values of T_c but also in a set of physical properties that cannot be described by the classical Bardeen–Cooper–Schriefffer (BCS) [7] scheme. In cuprates, charge carriers appear due to the doping of the CuO_2 planes of a parent antiferromagnetic insulator upon nonisovalent atomic substitution or the creation of oxygen vacancies in charge reservoirs outside the conducting planes. The distance between equivalent CuO_2 planes in neighboring unit cells is large compared to the in-plane distance between neighboring copper atoms, which results in a strong conductivity anisotropy at temperatures above T_c and the two-dimensional coherence of the superconducting state at temperatures below T_c.

1.1.1 Atomic Structure and Classification

CuO_2 planes plays a crucial role in superconducting in cuprate compounds. As shown in Table 1.1 crystal structure of cuprate compounds basically is tetragonal. Highest critical temperature reached in cuprates having flat and square CuO_2 planes. The CuO_2 planes in cuprates separated by the atoms as Bi, O, Y, Ba, La, etc. which plays role of charge reservoirs. In contrast to low temperature conventional

Table 1.1 Crystal structure and elementary cell of some cuprates [11]

Compounds	Crystal structure	Size of elementary cell,A	T_c, K
$La_{2-x}Sr_xCuO_4(La/Sr-214)$	Tetragonal	$a=b=3.78, c=13.2$	37.5
$YBa_2Cu_3O_7(123)$	Orthorhombic	$a=3.82, b=3.88, c=11.7$	90
$BiSr_2CaCu_2O_8(Bi-2212)$	Tetragonal	$a=b=5.4, c=30.89$	95
$TlBa_2Ca_2Cu_3O_9(Tl-1223)$	Tetragonal	$a=b=3.85, c=15.9$	120
$Tl_2Ba_2CuO_6(Tl-2201)$	Orthorhombic	$a=5.468, b=5.473, c=23.24$	90
$Tl_2Ba_2CaCu_2O_8(Tl-2212)$	Tetragonal	$a=b=3.86, c=29.3$	112
$Tl_2Ba_2Ca_2Cu_3O_{10}(Tl-2223)$	Tetragonal	$a=b=3.85, c=35.9$	125
$HgBa_2Ca_2Cu_3O_8(Hg-1223)$	Tetragonal	$a=b=3.85, c=15.9$	133
$HgBa_2Ca_3Cu_4O_{10}(Hg-1234)$	Tetragonal	$a=b=3.85, c=19$	127

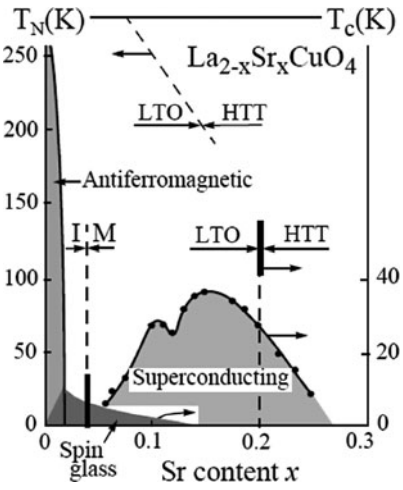

Fig. 1.1 Phase diagram of LaSrCuO (LSCO). As one can see in Fig. 1.1, Sr substitution for La in LSCO induces a structural phase transition from the high-temperature tetragonal (HTT) to low-temperature orthorhombic (LTO) and, at low temperatures, from the LTO phase to the low-temperature tetragonal (LTT) phase

superconductors, influence of carrier density on critical temperature $T_c(n)$ reveal nonmonotonic behavior [8]. There is an empirical expression of $T_c(n)$ dependence

$$T_c(n) \cong (T_c)_{\max} \left\{1 - 82.6(n - 0.16)^2\right\}, \tag{1.1}$$

where $(T_c)_{\max}$ is the maximum critical temperature for certain compound. Superconductivity occurs within the interval $0.05 \leq n \leq 0.27$, which vary slightly in different cuprates. In LaSrCuO compound at doping $x = \frac{1}{8}$, the curve $T_c(n)$ has a dip (Fig. 1.1). This dip is the so-called $\frac{1}{8}$ anomaly and inherent to $La_{2-x}Sr_xCuO_4$. The insulating phase occurs at $n \leq 0.05$ and usually called as an undoped region. The maximum critical temperature is observed at optimal doping $x \sim 0.16$ [9].

The most prominent compound $YBa_2Cu_3O_{7-\delta}$, the first high temperature superconductor discovered with a critical temperature T_c for the onset of superconductivity above the boiling point of liquid nitrogen, is traditionally abbreviated as "$YBCO$" or "$Y - 123$"($YBa_2Cu_3O_{7-\delta}$). The orthorhombic unit cell of $YBCO$ is presented in Fig. 1.2. The two CuO_2 layers are separated by a single Y atom. The replacement of yttrium by many of the lanthanide series of rare-earth elements causes no appreciable change in the superconducting properties. Each copper ion is surrounded by a pyramid of five oxygen ions. $YBCO$ is the only high temperature superconductor having the one-dimensional CuO chains. In $YBa_2Cu_3O_6$ CuO_2 chains are absent and this compound is the antiferromagnetic insulator [10]. So, oxygen content can be changed reversibly from 6.0 to 7.0 simply by pumping oxygen in and out of the parallel CuO chains running along the b axis. At low oxygen content, the lattice parameters $a \neq b$ (orthorhombic), while with increasing the oxygen content causes the unit cell to have square symmetry, $a = b$. At oxygen content of 6.4, the antiferromagnetic long-range order disappears and superconducting order parameter starts to grow. The maximum value of T_c is achieved at a doping level of about 6.95. From Fig. 1.3, we can see that at $x \sim 6.7$

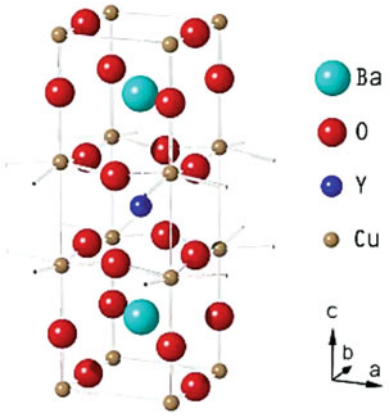

Fig. 1.2 Crystal structure of YBaCuO

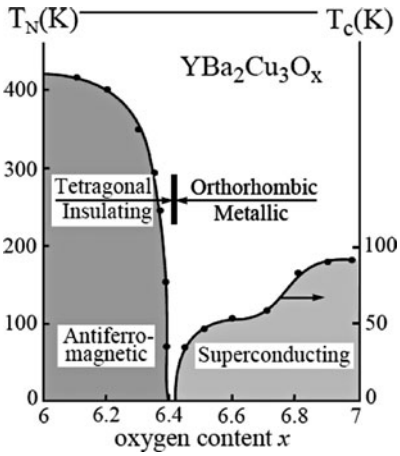

Fig. 1.3 Phase diagram of YBaCuO

there is plateau at $T_c \sim 60K$. One of the explanations of origin of this plateau is direct relation with $\frac{1}{8}$ anomaly observed in LaSrCuO.

In $Bi2212$ in unit cell the CuO_2 layer intercalated by Ca. The unit cell also contains two semiconducting BiO and two insulating SrO layers. The family of the bismuth cuprate consists of three members: $Bi2202$, $Bi2212$, and $Bi2223$ with the unit having 1, 2, and 3 CuO_2 layers, respectively. Critical temperature increases with increasing number of CuO_2 layers. The structure of the bismuth cuprates is very similar to the structure of thallium cuprates such as $Tl2202$, $Tl2212$, and $Tl2223$. In these compounds, bismuth replaced by the thallium, and strontium replaced by barium. Bismuth, thallium, and mercury cuprates have the lattice constants $a = b$, there is no twinning within a crystal.

In the Table 1.2 presented superconducting parameters of optimally doped cuprates: the coherence length $\xi_{ab,c}$ and London penetration depth $\lambda_{ab,c}$. As followed from the Table 1.2, cuprate superconductors reveals strong layered anisotropy of physical properties. In future investigations also important of introducing of

Table 1.2 Physical properties of cuprates [11]

Physical quantity	LSCO,A	YBCO,A	B2212,A	Hg1223,A
ξ_{ab}	33	15	20	13
ξ_c	2.5	2	1	2
λ_{ab}	2,000	1,450	1,800	1,770
λ_c	20,000	6,000	7,000	30,000

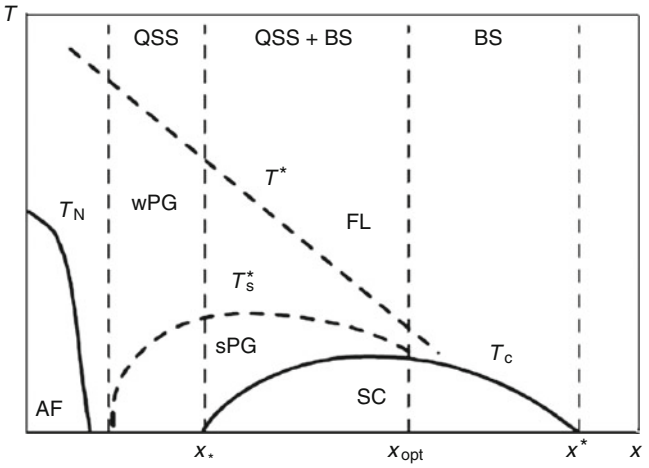

Fig. 1.4 Generalized phase diagram of the hole doped cuprate superconductors

anisotropy parameter of upper critical field $\gamma_{Hc2} = \frac{H_{c2,ab}}{H_{c2;c}}$. As shown by measurements for cuprate superconductors γ_{Hc2} changes in the interval 3–30 [11].

In the absence of an external magnetic field, the thermodynamic state of a doped cuprate compound can be described by the temperature T_c and the carrier concentration in the CuO_2 plane (doping level) x. In the phase diagram (Fig. 1.4), the superconducting state field corresponds to a certain doping range $x_* < x < x^*$ inside which the superconducting transition temperature reaches its maximum value at the optimum doping x_{opt}. Concentrations $x \leq x_{opt}$ correspond to underdoped cuprates, and concentrations $x \geq x_{opt}$ to overdoped cuprates. At $x \geq x_{opt}$ and $T > T_c$, cuprates are "bad" Fermi liquids, and at $x \leq x_{opt}$, over a wide temperature range $T_c < T < T_s^*$, they exhibit the pseudogap state, whose nature is unclear up to now [13]. The gap spectrum of quasiparticles at $T > T_c$ demonstrates that the superconducting phase appears from a certain insulating state rather than from a Fermi liquid, such that the ground states of an insulator and a superconductor, with similar structures and energies, converge near the superconducting transition line. This is indication of that strong correlations in cuprates is very important [14]. The pseudogap state is divided into a strong pseudogap that is adjacent to T_c and exists over a wide temperature range $T_c < T < T_s^*$, and a weak pseudogap between T_s^* and T^*. T_s^* corresponds to the breaking of a pair, and T_c corresponds to the appearance of phase coherence in the system of pairs. A consistent theory

of cuprate superconductivity should be able to explain both the high values of T_c and the physical properties of these compounds in a large neighborhood of the superconducting state that includes the strong and weak pseudogaps in the phase diagram.

1.1.2 Theoretical Models

Theoretical models for the explanation origin of superconductivity in cuprate superconductors can be divided into two groups. First group of models supports the origin of superconducting state from dielectric state [3, 4, 15–18]. Second group of theoretical approaches related with modification of classical electron–phonon coupling mechanism taking into account peculiarities of superconducting state in cuprate compounds [19, 20]. Strong electron correlations and the unusual symmetry of the pseudogap and the superconducting order parameter in cuprates are arguments for a purely electron superconductivity mechanism (rather than a phonon mechanism, as in the BCS or Eliashberg theory). The studies of this mechanism Hubbard model and the related $t-J$ model are described in a number of reviews (for example, see [18] and references therein). The two-dimensional Hubbard problem has not been exactly solved and approximate solutions obtained by numerical methods are often in conflict, which leads to reasonable doubts about the usefulness of this approach, especially because the unusual isotopic effect in cuprates [21–23] indicates a nontrivial role of phonons in pairing-interaction formation.

Another important moment in cuprate compounds is the growing of superconducting fluctuations [24]. Strong fluctuations can be described in framework of approach of the resonating valence bond [25, 26]. In accordance with resonating valence bond theory, the electrons which possess the opposite spins and located in the neighboring sites of the crystal lattice form pairs. At fixed temperature with decrease of the doping degree pairs are ordered in lattice and the state becomes antiferromagnetic. Vice versa, when the doping is fixed and temperature decreases, the pairs, being Bose particles, are condensed and the state becomes superconducting. The pseudogap manifests itself in the processes where the pair-breaking takes places. The Hamiltonian of Hubbard model has a form [15, 16]:

$$H_{\text{Hubbard}} = \sum_{ij} t_{ij} (c_{i\uparrow}^{+} c_{i\uparrow} + c_{i\downarrow}^{+} c_{i\downarrow}) + U \sum_{i} (c_{i\uparrow}^{+} c_{i\downarrow}^{+} c_{i\uparrow} c_{i\downarrow}), \tag{1.2}$$

where U Coulomb interaction in one site, t_{ij} tunneling integral between neighbor atoms, c^{+} and c creation and annihilation operators. Corresponding Hamiltonian for $t - J$ model can be written as [25]

$$H_{t-J} = \sum_{i\sigma} \varepsilon_0 n_{i\sigma} - \frac{1}{2} \sum_{i,i+\sigma} J(S_i^z S_{i+\delta}^z - n_i n_{i+\sigma}), \tag{1.3}$$

where S_i^z projection operator of spin, J effective exchange integral. Despite of the simple form of the Hamiltonians (1.2) and (1.3), the quantitative results allowing the experimental verification still have not been obtained in their framework. Probably, the $t - J$ model or of its modifications can describe the complete phase diagram presented in Fig. 1.4. No analytical solution of $t - J$ model still does not find and the characteristic value of J and x, separating different domains of the phase diagram, can be found only numerically. For the value $J = 0.3t$ numerical calculations was conducted in [27], and it was shown that the antiferromagnetic region restricted as $x < 0.1$. Some properties of the $t - J$ model or Hubbard Hamiltonian ground state can be found by means of the variational prosedure. In this way, the d-wave symmetry of the superconducting pairing was successfully obtained in [27,28]. Calculated in this way order parameter remains finite even at zero doping while the superfluid density n_s depends of the doping degree linearly [29]. In the typical phase diagram of hole-doped cuprates, the Neel (T_N) and superconducting transition (T_c) temperatures, respectively, bound the long-range antiferromagnetic and superconducting order regions. Strong pseudogap (sPG) and weak pseudogap (wPG) regions are separated by a crossover temperature T_s^*. The temperature T separates the weak pseudogap from the normal Fermi liquid (FL). The regions in which the bound states (BSs) and quasi-stationary states (QSSs) of pairs appear are shown, and the region of coexisting BS and QSS is also depicted.

In the case of overdoped and optimally doped high temperature superconductors, BCS type model can be useful for study cuprate superconductors. The paramagnon exchange between electrons results in their pairing. In contrast to the electron–phonon interaction in original BCS scheme, the electron (hole)–paramagnon interaction may be not weak. This leads to modification of BCS theory. The effect of soft paramagnons, with the characteristic energies small with respect to the pseudogap, on superconducting properties of high temperature superconductors became of the subject of work [30]. As shown in this study, influence of paramagnons is analogous to the effect of elastic impurities, which leads to the superconductivity with strongelectron–phonon coupling. Comparison paramagnon approach with the Migdal–Eliashberg [31, 32] theory was conducted in [30] and showed that despite the small ratios of electron to ion mass $\frac{m}{M}$ ratio justifying Eliashberg theory for phonons, an Eliashberg-type approach to the spin-fermion model is still allowed, but only at strong coupling [31].

The BCS superconducting instability of a Fermi system and Bose–Einstein Condensation (BEC) of bosons below a critical temperature can be unified by following the continuous evolution between these two limits as a strength of the fermion attraction increases. Within this approach, the phase diagram of cuprate superconductors can be interpreted in terms of a crossover from Bose–Einstein condensation of performed pairs to BCS superconductivity, as doping is varied. In the BEC limit, pairs form at high temperatures as result of strong coupling, and condense at some lower temperature, while in the BCS limit pairs form and condense at the same temperature. A large amount paper is devoted to the development of this idea [33–36]. The existence of pairs above T_c is the characteristic feature of a BEC

condensation, but their direct detection is so far an unsolved experimental problem. Other, fewer direct signatures of this mode of condensation that have been quoted in the literature include the power law dependence of T_c on the penetration depth λ, $T_c \sim \lambda^{-2}$, interpreted as being due to the way the superfluid density n_s varies with doping,

$$T_c \sim \frac{n_s}{m^*}, \tag{1.4}$$

assuming the effective mass m^* to be constant [37]. Another important moment is the existence of isotope effect on the pseudogap temperature T^*.

One of the popular scenario of theory of superconductivity in cuprate compounds is the bipolaron mechanism. In this model, electrons are coupled strongly in bipolarons [38] due to the electron–phonon interaction which is supposed to be with the characteristic energy considerably exceeding the Fermi energy. As a result, the mobile bipolarons are formed in normal state with their further Bose–Einstein condensation [38].

There are also purely phenomenological models in addition to above-mentioned semi-phenomenological models. These models related with a phenomenological description of the fermionic subsystem are possible after integration over all Bose fields. The first of such models is the marginal Fermi liquid model [39]. In this approach, the one-electron Green function has a usual form

$$G(\mathbf{k}, \omega) = \frac{1}{\omega - \varepsilon(\mathbf{k}) - \sum(\mathbf{k}, \omega)}, \tag{1.5}$$

but self-energy part $\sum(\mathbf{k}, \omega)$ has an unusual structure [39]. Marginal Fermi liquid theory allows explaining the series of cuprate normal state anomalies, including the linear resistivity, specific heat peculiarities, a.c. conductivity. Another purely phenomenological model related with generalization GL theory, including both superconducting and antiferromagnetic fluctuations were taken into account [40]. This model also is called SO(5) model [40]. In this approach, five-dimensional order parameters were introduced for describing superconductivity and antiferromagnetism together. Speaking about phenomenogical model is necessary to underline that GL remains a very effective method for study superconductivity. In future chapters, we will discuss different versions of GL equations and their application for unconventional superconductors.

One of the main and the most evident contradictions between theory and experiment was the linewidth of the Angle Resolved Photoemission (ARPES) peak in undoped cuprates. Although the dispersion of the peak is well reproduced by $tt't''-J$ model, its width is very broad in experiment [41] and very narrow in theory [42]. Naively, contribution of electron–phonon interaction cannot explain the large width since the coupling to phonons, in addition to broadening, must also change the dispersion of the particle which, in turn, is already well described by the pure $tt't''-J$ model. However, as was shown in [43,44], in the strong coupling regime of electron–phonon interaction the situation is exactly the same as in experiment. The

polaron quasiparticle has very small weight and cannot be seen in experiment while shake-off Frank–Condon peak completely reproduces the dispersion of the pure magnetic model without electron–phonon interaction. Naturally, in such case the chemical potential must be pinned not to the observed broad shake-off peak but to the real invisible quasiparticle. Such decoupling of the chemical potential from the broad peak was observed in experiment [45] a few months after prediction had been made in [46].

Understanding the nature of the ground state and its low-lying excitations in the cuprate superconductors is a prerequisite for determining the origin of high temperature superconductivity. A superconducting order parameter with a predominantly $d_{x^2-y^2}$ symmetry is well established [47, 48]. However, there are several important issues that remain highly controversial. For example (in hole-doped compound such as $YBCO$), various deviations from a pure d-wave pair state, such as the possibility of Cooper pairing with broken time-reversal symmetry or an admixed $d_{x^2-y^2}+s$ symmetry have been theoretically predicted [49, 50] and actively sought in numerous experimental studies [51, 52]. Furthermore, a transition of the pairing symmetry from d-wave behavior to s-wave-like behavior was also suggested as function of doping and temperature in various electron doped compounds [53, 54].

Further theoretical and experimental studies brought more evidences of the importance of electron–phonon interaction in cuprates. One of the evidences is the two-peak structure of the mid infra-red part of optical conductivity in the underdoped compounds, which is easily reproduced by taking the electron–phonon interaction into account [46]. Another confirmation is the anomalous temperature dependence of the width of the ARPES peak which can be explained only by the interplay of magnetic and lattice system [55, 56]. Various estimates for the electron–phonon interaction strength give the value $\lambda \approx 1$ for undoped compounds [55, 57, 58]. The strength of electron–phonon interaction decreases with an increase of the concentration of holes reaching the intermediate coupling regime at optimal doping [46, 58]. In [59], the isotope effect in the $Y_{1-x}Pr_xBaCu_3O_{7-d}$ compound in all phases (superconducting, spin glass, and anti-ferromagnetic) was reported. Although somewhat debatable, there is experimental evidence [60] that electron–phonon interactions can be used to explain the fundamental mechanism operating in high-temperature cuprate superconductors. The dependence of the isotope shift parameter $\alpha_0 = -\frac{d \ln T_c}{d \ln M}$ on the carrier density in cuprate superconductors is presented in Fig. 1.5.

As shown in [11, 12, 60] in underdoped compounds isotope shift parameter is at the level 0.3. The existence of a strong electron–phonon interaction in cuprate superconductors was confirmed by the observation of a subgap structure in tunnel Josephson junction experiments [61]. As discussed in [62], similar phenomena occur due to the interaction of a Josephson current with phonons. As shown very recently in [63, 64], the electron–phonon mechanism explains many features of the low-energy relaxation process in cuprate superconductors, including the high values of the critical temperature; however, there are problems of coexistence of electron–phonon mechanism and unconventional symmetry of an order parameter.

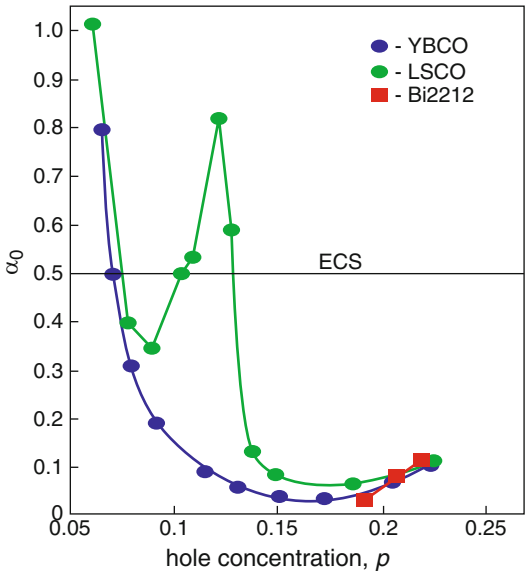

Fig. 1.5 Isotope shift parameter $\alpha_0 = -\frac{d \ln T_c}{d \ln M}$ versus carrier density in cuprate superconductors [12]

1.2 Borocarbides

The other class of new superconductors is rare-earth transition-metal borocarbides with the formula RNi_2B_2C (more general formula $RTBC(N); T-$ transition metal), which attracted the interest of many researchers, because of their wide variety of physical properties: compounds with $R = Lu, Y$ exhibit fairly high superconducting transition temperatures, T_c, of about 15–16 K [65]; magnetism coexists with superconductivity for $R = Dy, Ho, Er$ and Tm [66]; whereas the only antiferromagnetic order occurs for $R = Pr, Nd, Sm, Gd$ and Tb [67]. These compounds show a layered structure, and therefore they are considered as possibly close to quasi-two-dimensional cuprates. However, various local density approximation band structure calculations [68–71] clearly indicated the three-dimensional electronic structure. Quantum oscillation measurements of nonmagnetic borocarbides $LuNi_2B_2C$ and YNi_2B_2C give clear evidence for a multiband character in the normal state [72]. The value of the gap ratio $\frac{2\Delta}{T_c}$ varies from 0.45 to 3.2 [73–75]. d-wave model of superconductivity was proposed for nonmagnetic borocarbides YNi_2B_2C and $LuNi_2B_2C$ for explanation of anisotropy effects [76, 77].

As mentioned by many authors, superconductivity in these materials is caused by phonons, as evidenced by specific heat [78, 79] and isotope effect [80, 81] measurements. It would then appear natural to relate the suppression of superconductivity, as R and the transition metal (T) are varied, in terms of the BCS parameters, $\omega_D, N(E_F)$ and V (respectively, the Debye temperature, the density of states at the Fermi level, and some measure of the electron–phonon coupling strength):

$$T_c = \omega_D e^{-\frac{1}{N(E_F)V}}. \tag{1.6}$$

Table 1.3 Some superconducting characteristics of nonmagnetic borocarbides $LuNi_2B_2C$ and YNi_2B_2C [90]

Physical property	YNi_2B_2C	$LuNi_2B_2C$
$T_c(K)$	15.5	16.5
$H_{c2}(0)(T)$	11	12
$H_{c1}(0)(mT)$	20–30	60
$\xi(0)(A)$	55	65
$\lambda(0)(A)$	1200	800
$\kappa(0) = \lambda(0)/\xi(0)$	22	12
$\Delta C(mJ/mol/K)$	460	495
$\Delta C/\gamma T_c$	1.83	2.1
λ_{e-ph}	1	1.2

Since resistivity measurements indicate that V does not vary much with R in RNi_2B_2C [82], one is left primarily with ω_D and $N(E_F)$. While ω_D generally increases as R goes from Lu to La, measurements of the Sommerfeld coefficient, $\gamma \propto N(E_F)$, lead to $\gamma_{Lu} \sim 2\gamma_{La}$ in the Ni series. However, as the transition metal is varied, this simple parametrization no longer accounts for the trend of experimental data in an unambiguous way. Indeed, $LaPt_2B_2C$ is a superconductor [and, for this Pt series, so are the compounds with $R = Pr, Y$ [83], and, possibly [84], Nd], even though it has a smaller $N(E_F)$ than nonsuperconducting $LaNi_2B_2C$: $\gamma = 5 - 8\,\mathrm{mJ/molK}^2$, respectively [85].

There are any indications for unconventional pairing in nonmagnetic compounds $LuNi_2B_2C$ and YNi_2B_2C. Below presented list of several properties: **a)** a nonlinear $H^{1-\beta}$ -dependence of the electronic specific heat in the superconducting state instead of the standard linear dependence**, b)** weak damping of the de Haas–van Alphen oscillations in the superconducting state, which can be related with vanishing gap at the parts of the Fermi surface [86]. **c)** a nonexponential and nonuniversal character of the temperature dependence of the electronic specific heat

$$C_{el} \sim T^{\beta}, \tag{1.7}$$

with $\beta \sim 3$ at low temperatures (in YNi_2B_2C we have $\beta \approx 3$ [87], $\beta > 3$ for $LuNi_2B_2C$ and $LaPt_2B_2C$) **d)** the anisotropy of upper critical field within basal plane of $LuNi_2B_2C$ [88] **e)** a quadratic flux line lattice at high fields has been observed not only for magnetic borocarbides but also for nonmagnetic compounds [89] **f)** deviations from the Korringa behavior of the nuclear spin lattice relaxation rate $\frac{1}{T_1T} = const$ have been ascribed to the presence of antiferromagnetic spin fluctuations on the Ni site. Fundamental superconducting state parameters of nonmagnetic borocarbides $Y(Lu)Ni_2B_2C$ presented in Table 1.3.

The coexistence or competition of magnetism and superconductivity in borocarbides with magnetic rare earth elements is one of the most challenging problems in the field. Most dramatic effects have been observed for $HoNi_2B_2C$, where below the onset of superconductivity at 8.8 K a suppression of superconductivity for magnetic field perpendicular top the c-axis and $4.5 < T < 5.5K$ has been observed in [91]. There are three magnetic structures shown in this region: c-axis modulated commensurate cc, the spiral c-axis modulated incommensurate icc

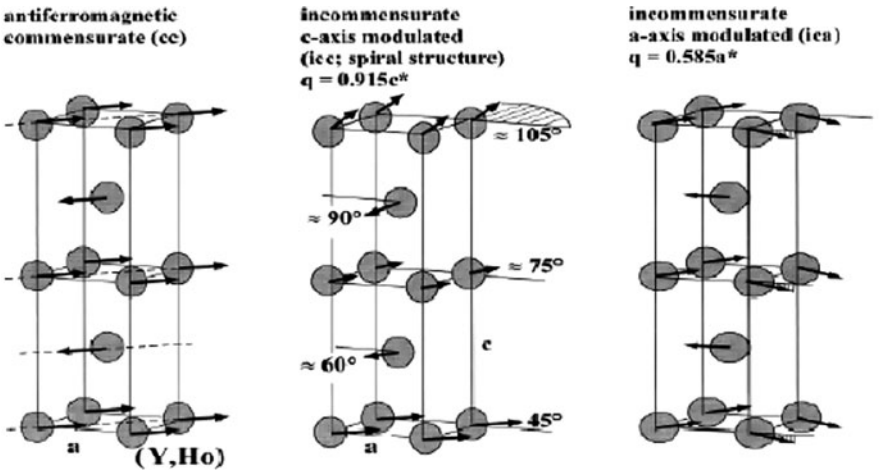

Fig. 1.6 Magnetic structure observed for the compound $HoNi_2B_2C$

and a-axis modulated incommensurate *ica* ones. From the fact the *icc* structure and the superconductivity both occur within a narrow temperature range and that these effects have only been observed for $HoNi_2B_2C$, it has been supposed that the *icc* structure is the origin for the superconductivity (Fig. 1.6). However, replacing Ho partially by the nonmagnetic Y, the magnetic structures for $Y_{1-x}Ho_xNi_2B_2C$ are shifted differently to lower temperatures. This has enabled researchers [92] to identify the ica phase as the one responsible for the superconductivity phenomenon. The observed vector in the a-modulated incommensurate structure $Q = 0.585a^*$ is close to the above-mentioned calculated nesting vector of $0.6a^*$. A phenomenon, sometimes observed, is the so-called reentrant superconductivity, i.e., for decreasing temperature first material becomes superconducting and the a transition into the normal state observed before, at lower temperature, the superconducting state is reached again [92]. Influence of the interplay between helicoidal magnetic ordering and superconductivity on the differential conductance in $Ho(NiB)_2C/Ag$ junctions was investigated in [93, 94].

Magnetic ordering in RNi_2B_2C compounds may result in a structural distortion caused by magnetostatic effects. Using high-resolution neutron scattering on a powder sample of $HoNi_2B_2C$, a tetragonal-to-orthorhombic distortion has been observed at low temperatures, where the Ho magnetic moment order in a c-axis modulated antiferromagnetic structure. Distortion is a shortening of the tetragonal unit cell in [110] direction. At 1.5 K, this shortening is 0.19% [95]. a similar tetragonal- to-orthorhombic phase transition driven by magnetostatic interaction has been also reported for $ErNi_2B_2C$ [96]. The different types of antiferromagnetic order in RNi_2B_2C compounds have been determined by neutron diffraction [97]. The large variety of antiferromagnetic structures and the fact that in most cases they are not simple commensurate structures is related to the competition of crystalline electric field with Ruderman–Kittel–Kasuya–Yoshida exchange interaction, the modulation of which is not commensurable with the lattice structure. Now, it is

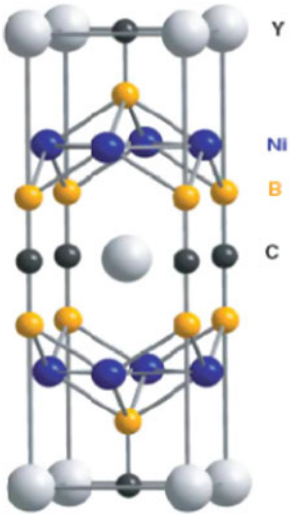

Fig. 1.7 Crystal structure of YNi_2B_2C

generally accepted that the RNi_2B_2C compounds are three dimensional in their behavior, and thus are, in fact, quite different than the layered cuprates.

1.2.1 Crystal Structure and T_c

The tetragonal layered crystal structure of the $I4/mmm$ or $P4/nmm$ types resolved so far for all well-characterized $RTBC(N)$ compounds can be written schematically as $(RC(N))_n(TB)_2$ with $n = 1, 2, 3$. (Fig. 1.7). There are systematic dependences of critical temperature T_c with increasing $T-T$ distance, the transition metal component T: Ni, Pd, Pt and the dopants replacing the T: Cu, Co, V, etc., and the $B-T-B$ bond angle. Finally, the number of metallic layers separating and doping the $(NiB)_2$ networks also has a profound effect on the actual T_c value. Thus, for the single RC-layer ($T = Ni$) compounds the highest $T_c \approx 14$ to $16.6K$ values are obtained for $R = Sc, Y, Lu$, whereas for $R = Th$ it is reduced to $8K$ and it vanishes for $R = La$. The double-layer Lu, Y-compounds exhibit very small transition temperatures of 2.9 K and 0.7 K [98], respectively, which however can be increased considerably replacing Ni by Cu [99]. In the case of the two-layer boronitride $(LaN)_2(NiB)_2$, triplelayer and quadro-layer $(YC)_2(NiB)_2$ so far no superconductivity has been detected, whereas the corresponding triple-layer compound exhibits a relatively high $T_c \approx 12K$.

1.2.2 The Electronic Structure

A typical band-structure calculation reveals sizeable dispersion in c-direction of the bands crossing the Fermi level and fluctuation magnetoconductance measurements clearly demonstrate the three-dimensional nature of the superconductivity under

consideration. Electronically, the coupling of the two-dimensional -$(TB)_2$ networks is mediated mainly by the carbon and boron $2p_z$ states. Further, important issues are the peak of the density of states $N(0)$ near the Fermi level $E_F = 0$ and the intermediate strength of correlation effects [100]. The electronic structure near $E_F = 0$ of all $RTBC(N)$ compounds is characterized by a special band complex containing three or four bands total width about 1 eV, for the case of $LaPtBC$. Compared with YNi_2B_2C and $LuNi_2B_2C$ for most of the other $RTBC$ superconductors density of state near Fermi level are reduced. The comparison with the available specific heat data predicts that most $RTBC(N)$ compounds exhibit intermediately strong averaged electron–phonon interaction $\lambda_{el-ph} \sim 0.5$ to 1.2, except $LaT_2B_2C, T = Ni, Pd$, which are weakly coupled and take place effect of pairbreaking.

Physical properties such as the Hall conductivity, de Haas–van Alphen frequencies and related data, as well as the upper critical field $H_{c2}(T)$ are strongly determined by the shape of the Fermi surface. Band-structure of nonmagnetic borocarbides YNi_2B_2C and $LuNi_2B_2C$ was calculated in [68–70]. Corresponding Fermi surface of $LuNi_2B_2C$ is shown in Fig. 1.8 [67]. Fermi surfaces of both nonmagnetic compounds exhibit a similar geometry, characterized by a strong anisotropic behavior and special nestedregions along the a direction with vector $\mathbf{q}_n \sim 0.5$ to $1.2\frac{\pi}{a}$. Nested and anisotropic properties for the Fermi surface of $LuNi_2B_2C$ close to the prediction [67]. Such topology has been observed by electron–positron annihilation radiation [101]. Very useful information about normal state of nonmagnetic borocarbides can be obtained from de Haas–van Alphen experiments [102]. In high quality YNi_2B_2C crystals, six cross sections are found. The related Fermi velocities on extremal orbits can be grouped into two sets differing by a factor 4. These observations and sizeable anisotropy of the H_{c2} for such crystals clearly indicate they are nearly in clean-limit regime.

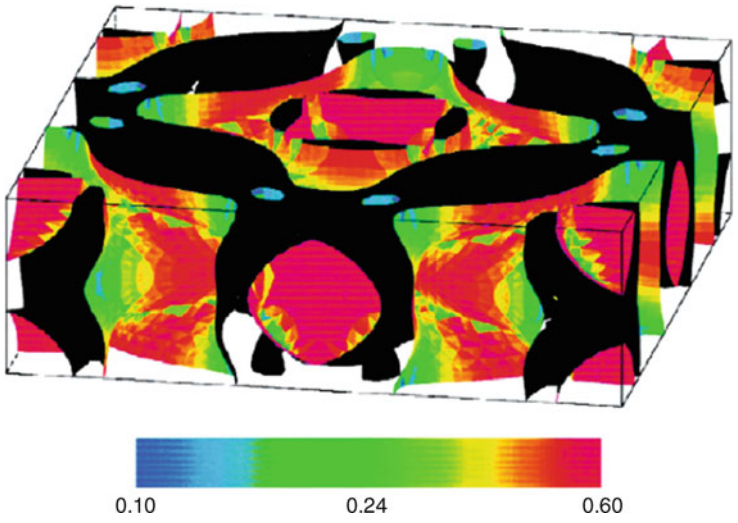

Fig. 1.8 Fermi surface of nonmagnetic borocarbide $LuNi_2B_2C$. The magnitude of Fermi velocity v_F given at bottom

1.3 Magnesium Diboride

MgB_2 was discovered to be superconducting only in 2001 year [103], and despite that many of its characteristics have now been investigated and a consensus exists about its outstanding properties. First of all, this refers to its high $T_c \approx 40K$), which is a recordbreaking value among the $s - p$ metals and alloys. It appears that this material is a rare example of the multi-band (at least two) electronic structures, which are weakly connected with each other. These bands lead to very uncommon properties. For example, T_c is almost independent of elastic scattering, unlike for other two-band superconductors [104]. Additionally, MgB_2 has high potential to replace conventional superconducting materials in the electronic applications. Large critical densities are already reported for bulk samples [105] and bulk superconductivity is established immediately to support supercurrent transport between grains [106]. The material shows a pronounced isotope effect [107]. Measurements of the nuclear spin-lattice relaxation rate [108] indicate that MgB_2 is a BCS type phonon-mediated superconductor. Calculations of the band structure and the phonon spectrum predict double energy gap [109, 110], a larger gap attributed to two-dimensional p_{x-y} orbitals and smaller gap attributed to three-dimensional p_z bonding and anti-bonding orbitals. The maximal upper critical magnetic field can be made much higher than that for a single-band dirty superconductor [111]. The properties of MgB_2 have been comprehensively calculated by the modern theoretical methods, which lead to a basic understanding of their behavior in various experiments.

Any kind of disorder potentially changes the properties of MgB_2. Disorder can be introduced in a controlled way by doping or irradiation, but often arises from the preparation conditions [112]. Disorder generally decreases the transition temperature [112]. It has been suggested that intrinsic properties are affected by: (i) macroscopic particles that contribute to lattice distortion enhance both and scattering, (ii) disorder in the Mg sublattice (e.g., by Al addition) can increase the scattering, (iii) oxygen or carbon when substituting for B is expected to provide strong scattering [113, 114]. Superconductivity in the π-band is suppressed at high magnetic fields, where the σ-band determines the magnetic properties and MgB_2 behaves as a single-band superconductor [112]. The σ-band contributes significantly to the condensation energy and to the superfluid density only at low magnetic fields (below about 1 T in clean materials) [112]. Clean grain boundaries are no obstacles for supercurrents in MgB_2 [112, 115–117]. This advantage compared to high temperature superconductors allows simple preparation techniques, but, the connections between the grains remain delicate, since dirty grain boundaries potentially reduce the critical currents [116, 118]. The main properties of MgB_2 are presented in Table 1.4.

Study of core structure of a single vortex in two-band superconductors was conducted in [120]. As shown in this work, at low temperatures a Kramer–Pesch effect occurs, i.e., a shrinkage of the size of the vortex core. Interestingly, this core shrinkage even exist, if only the σ band is in the clean limit. This situation is believed to be realistic for high-quality MgB_2 samples and opens the possibility to observe

Table 1.4 Some superconducting characteristics of MgB_2 [119]

Parameters	Values
Carrier density (holes/sm^3)	$(1.7–2.8) \times 10^{23}$
Isotop shift	0.32
$H_{c2}^{ab}(0)(T)$	14–39
$H_{c2}^{c}(0)(T)$	2–24
$H_{c1}(0)(mT)$	17–48
$\xi_{ab}(0)(nm)$	3.7–12
$\xi_{c}(0)(nm)$	1.6–3.6
$\lambda(0)(nm)$	85–180

the Kramer-Pesch effect in this compound [121]. The temperature dependence of the microwave conductivity in MgB_2 thin films at a fixed microwave frequency shows a peak at temperatures around $0.5T_c$ [122]. This is in contrast to conventional superconductors where a peak close to T_c appears and also in contrast to the cuprates where a huge conductivity peak at very low has been observed [123].

Another peculiarity of two-band superconductors is the occurrence of Leggett mode, which related with collective mode of small fluctuations of relative phase of the two superconducting order parameter [124]. Expression for Leggett mode*s* in MgB_2 given by the expression [125]

$$\omega_0 \sim 2\left[\frac{\Delta_\sigma \Delta_\pi(\lambda_{12}+\lambda_{21})}{\lambda_{11}\lambda_{22}-\lambda_{12}\lambda_{21}}\right]^{1/2}, \tag{1.8}$$

where λ_{ij} is the interband and intraband electron–phonon interaction parameters. As followed from Exp.(1.8), Legget modes is determined by the interband interaction parameters and is absent in the case noninteracting bands. This mode is observable if $\omega_0 < 2\Delta_\pi$ [125]. Experimental investigation of Legget modes conducted in $Al_xMg_{1-x}B_2$ [126] using Andreev spectroscopy method.

1.3.1 Crystal Structure

Magnesium diboride, like other diborides MeB_2 ($Me = Al, Zr, Ta, Nb, Ti, V$ etc.), crystallizes in a hexagonal structure, where honeycomb layers of boron are intercalated with hexagonal layers of magnesium locate above and below the centers of boron hexagons (Fig. 1.9). The bonding between boron atoms is much stronger than that between magnesium, and therefore the disordering in the magnesium layers appears to be much easier than in the boron layers. This difference in bonding between boron and magnesium atoms hinders the fabrication of MgB_2 single crystals of appreciable size. Despite crystal structure of MgB_2 being similar to that of a graphite intercalated compounds, MgB_2 has a qualitatively different and uncommon structure of the conducting states.

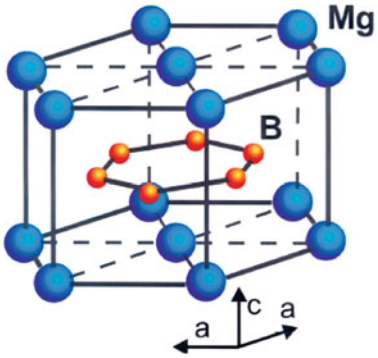

Fig. 1.9 Crystal structure of MgB_2

1.3.2 Electronic and Band Structure

The electron band structure of MgB_2 has been calculated using different ab initio methods yielding basically the same result [109, 111, 127–129]. The dispersion relations for boron p_z character orbitals, which play a major role in transport and thermodynamic properties. The radii of the hollow circles are proportional to the π-band character, which is made from p_z boron orbitals, while those of the filled circles are proportional to the σ-band character, made from p_{xy} orbitals. The most important is a quasi two-dimensional dispersion relation along the ΓA (Δ) direction with a small Fermi energy $\approx$ $0.6eV$, and accordingly, with a moderate Fermi velocity. The corresponding sheets of the Fermi energy form the cylindrical surfaces along the ΓA direction seen in Fermi surface for MgB_2 (Fig. 1.10). The corresponding electron transport is very anisotropic (ρ_c/ρ_{ab} $\approx$3.5 [130]) with the plasma frequency for the σ- band along the c (or z) axis being much smaller than that in the ab (xy) direction [131]. The hole branch along ΓA (Δ) experiences a huge interaction with the phonon E_{2g} mode for carriers moving along the ab plane, although its manifestation is screened effectively by the much faster hole mobility in the π-band [104].

An investigation of the charge density distribution would give a better understanding of how the superconductivity is related to the electronic and crystal structure MgB_2. Precise X-ray structure analysis [132–134] yielded accurate charge densities in MgB_2. The vortex density obtained at room temperature revealed a strong $B-B$ covalent bonding feature. On the other hand, there was no bond electron between Mg and B atoms, and Mg atoms were found to be fully ionized and in the divalent state. As shown in [132], the value for Mg atoms is very close to the number of electrons around Mg^{2+} ions, so Mg atoms are fully ionized in the MgB_2 crystal at whole temperatures. On the other hand, the total numbers of electrons around boron two-dimensional sheets show significant difference, which can be attributed to the valence of the whole boron two-dimensional sheet changing from neutral to monovalent at $15K$. This result suggests that the electrons transfer from π band (p_z orbitals) to interplane σ band (p_{xy} orbitals) at $15K$.

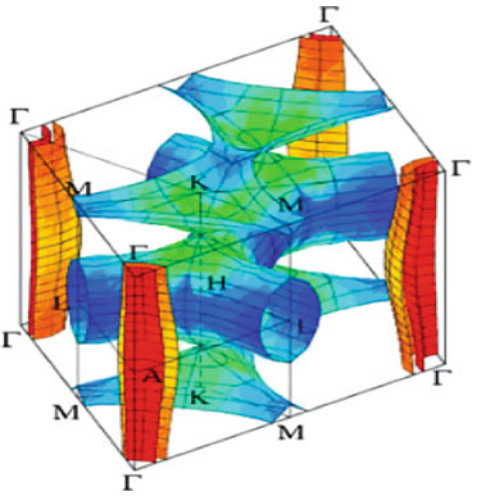

Fig. 1.10 Fermi surface of MgB_2

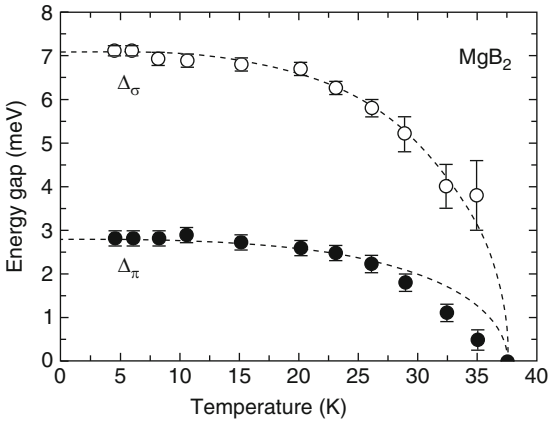

Fig. 1.11 Experimentally measured two-gaps in MgB_2

Various theoretical and experimental problems of the family of doped MgB_2 relative compounds are also widely investigated. The behavior of the superconducting gaps with doping seems interesting. The experimental situation can be followed [135, 136]. Theoretical study of superconductivity in doped MgB_2 compounds was conducted in [137–140]. Last model applied for calculation in $Al_xMg_{1-x}B_2$. The experimentally observed suppression of the σ band gap is reproduced, whereas the three-dimensional π band gap shows no essential change until $x = 0.4$. The $\sigma - \pi$ bands crossing appears at $x_c = 0.485$ where $\Delta_{\sigma,\pi}(0) = 1.09\, meV$. Further, the gap decreases rapidly and vanish at the same T_c in accordance with the presence of interband pairing channel. The measured value for the merging point of the gaps is $x_c = 0.34$ [141]. The leading σ gap depression reflects the deviation from the optimal "self-doping" of pure MgB_2, which weakens the σ intrabandpairing. Near x_c the dimensionality of the σ band changes as also the chemical potential relation to the bands. The ratio $\frac{\Delta_\sigma}{\Delta_\pi}$ calculated by [140] seems to fall off to slowly as compared with the measurement (Fig. 1.11) [136].

1.4 Oxypnictides

In 2008, superconductivity at 26 K in the oxypnictide compound $LaFeAs(O, F)$ was discovered [142]. The first communication on the superconductivity of $LaOFeAs$ appeared as early as 2006, but the temperature T_c of the superconducting transition proved to be low, $T_c = 3.5K$. Similarly, for LaONiP, $T_c = 4.5K$ was obtained [143]. Later, by substituting other rare-earth elements for La, several groups obtained considerably higher values ($T_c = 41K$ in $CeO_{1-x}F_xFeAs$ [144], $T_c = 52K$ in $PrO_{1-x}F_xFeAs$ [145]) and reached $T_c = 55K$ in $SmO_{1-x}F_xFeAs$ [146]. The parent compounds exhibit antiferromagnetic ordering of the iron moments, which are suppressed by doping in favor of superconductivity. The early awareness that magnetic order, even if in competition with superconductivity, is a key factor for determining superconductivity, drove the discovery within a short period of new iron-based superconductor families with different crystal structures such as $(Ba, K)Fe_2As_2$ [147], $LiFeAs$ [148] and $FeSe$ [149]. A large number of different compounds have now shown that superconductivity can be induced by carrier doping, both in the $Fe - As$ layer and in the spacing layer, and by external as well as by internal pressure. For simplicity in the following we will refer to the different families as: 1111 ($REFeAs(O, F)$), 122 ($(Ba, K)Fe_2As_2$), 11 $Fe(Se, Te)$), 111 ($LiFeAs$) [150, 151].

A phase diagram on the plane $T - x$ typical of the compounds of this type is shown in Fig. 1.12 [152]. This diagram resembles the diagrams characteristic of the cuprate superconductors, e.g., $La_{2-x}Sr_xCuO_4$. In cuprates, the superconductivity appears in compounds of the La_2CuO_4 type as lanthanum is replaced by strontium. In both systems, the doping introduces charge carriers (electrons or holes), which suppresses the antiferromagnetic ordering and creates conditions for Cooper pairing. This analogy has led to the assumption that the high-temperature superconductivity of the new $FeAs$-type superconductors is caused by the proximity of the system

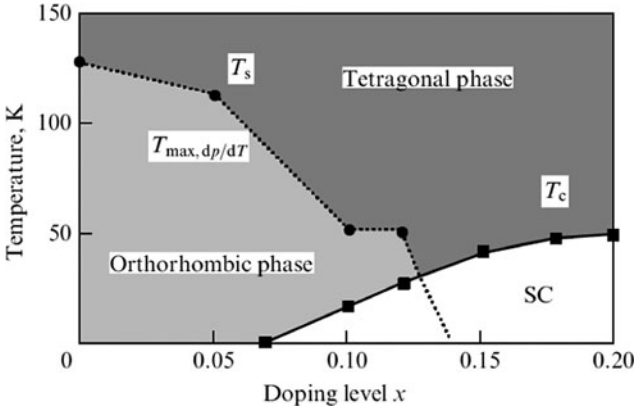

Fig. 1.12 Typical phase diagram of $REO_{1-x}F_xFeAs$ compounds (RE is a rare-earth element) on the (T; x) plane. T_s is the structural transition temperature

to the magnetic phase transition; in this case, high values of T_c are caused by the pairing of charge carriers through spin fluctuations. In doped AFe_2As_2 compounds, superconductivity at $T_c = 38K$ was revealed immediately [147].

This assumption is confirmed by many detailed physical studies. The results of calculations of the electron–phonon coupling in these compounds showed that the high values of T_c in these new compounds cannot be explained in terms of the standard electron–phonon pairing mechanism. Using ab initio calculations of electron and phonon spectra for *LaOFeAs* was performed in [153]. Taking into account the value of the average logarithmic frequency of phonons [153] and neglecting Coulomb pseudopotential, Allen–Dynes formula [154, 155] gives the value of $T_c = 0.5$ K. In this study, numerical solution of Eliashberg equations with the calculated electron–phonon interaction function $\alpha^2\ F(\omega)$ was used [153, 154]. Actually, to reproduce the experimental value of $T_c = 26$ K, coupling constant λ should be approximately five times larger, even Coulomb repulsion is zero.

It is well known that electron–phonon mechanism in Cooper pairing was always considered to be the observation of the isotope effect. Appropriate measurements were performed recently in [156] on $SmFeAsO_{1-x}F_x$, where ^{16}O was replaced by ^{18}O, and on $Ba_{1-x}K_xFe_2As_2$, where ^{54}Fe was substituted for ^{56}Fe. A finite shift in superconducting transition temperature was observed, which can be characterized in a standard way by the isotope effect exponent $\alpha_0 = -\frac{\ln T_c}{\ln M}$. For $SmFeAsO_{1-x}F_x$, the isotope effect turned out to be small enough, with $\alpha_0 \approx 0.00$, which is quite natural as O ions reside exterior to the conducting *FeAs* layer. At the same time, the replacement of Fe ions in *FeAs* layers in $Ba_{1-x}K_xFe_2As_2$ has led to a large isotope effect with a 0.4, which is close to the "ideal" value of 0.5.

A superconductivity mechanism relying on the occurrence of nonmagnetic bipolaron in doped oxypnictides was proposed in [157] based on the Bose–Einstein Condensation of the bipolarons (see also [158, 159]). The applicability of another, so-called hole mechanism of superconductivity (see [160]) to the description of oxypnictides is analyzed in [161]. A "universal" superconductivity model proposed in [162] implies pairing of electrons with parallel spins and the existence of distinguished charge and magnetic bands (vortex lines) in oxyarsenides; this model was used to describe the effect of external pressure on the transition temperature. In [163], this model was used to calculate the optimum doping level of superconducting oxyarsenide. A possible superconductivity mechanism, including the electron–electron and electron–hole pairings as the respective consequence of electron–phonon and Coulomb interactions is reported in [164].

After a comparison among the families 122 comes out the most suitable for application with rather high T_c, upper critical field, low anisotropy, reduced thermal fluctuations and intrinsic pinning mechanisms. In particular, the Co-doped 122 compound with T_c of ~22 K $H_{c2}(0)$ of greater than 50 T, has almost twice that of Nb_3Sn (30 T) with a T_c of 18 K. Although the Nb-base materials are isotropic, Co-122 is almost isotropic ($\gamma_{Hc2} < 2$) too, making it potentially competitive as a low temperature superconductor. Even the highest T_c pnictides, Sm- and Nd-1111 have anisotropies much smaller than typical cuprates ($\gamma_{Hc2} \sim 30$). However, a typical YBCO has $\gamma_{Hc2} \sim 5$, similar to the 1111. A clear drawback to present applications of the pnictides is their extrinsic and perhaps intrinsic granularity that

Table 1.5 Some superconducting characteristics of oxypnictides [165]

Physical property	Nd-1111	Ba122	Fe11
$T_c(K)$	47.4	22.0	14.5
$\mu_0 dH_{c2}^c/dT(T/K)$	2.1	2.5	14
$\mu_0 dH_{c2}^{ab}/dT(T/K)$	10.1	4.9	26
γ_{Hc2}	5	1.9−1.5	1.9−1.1
$\xi_{ab}(nm)$	1.8	2.4	1.2
$\xi_c(nm)$	0.45	1.2	0.35
Gi, Ginzburg number	0.008	0.00017	0.0013

significantly restrict the critical current density of polycrystalline forms. However, only few years have passed since the first reports of T_c above 20 K in the pnictides, we should not expect that discoveries are yet over or that the final word on applications can yet be given. The main properties of oxypnictides are presented in Table 1.5.

As mentioned above, phase diagrams on the $T - x$ plane, where x is the concentration of the dopant (Fig. 1.12), are very similar to cuprate superconductors. Nevertheless, there is an essential difference between the cuprates and $FeAs$ systems caused by electron correlations. Doped cuprate superconductors, in contrast to $FeAs$ systems, are near the Mott–Hubbard metal-insulator transition, although in both cases superconductivity appears near the transition to the antiferromagnetic state. This means that the cuprates belong to materials with strong electron correlations, whereas $FeAs$ systems are weakly (or moderately) correlated materials, although this question is still under discussion. But there is an essential difference between $FeAs$ systems and the cuprates, which lies in the fact that the initial (stoichiometric) compounds are insulators in the case of cuprates and metals in $FeAs$ systems. In both cases, however, the initial compounds are antiferromagnetic, although with localized magnetic moments in the first case and with itinerant-electron magnetism in the second. Upon doping the initial compounds, the temperatures of magnetic ordering T_N decrease sharply and the compounds become superconducting at concentrations of a dopant of the order of 10%. The doping creates charge carriers in the main layers, which determine the interesting physics in cuprate materials. In the new class of oxypnictides, as in the cuprates, the doping can create either electrons or holes in the main layer. Depending on the relation between the valences of the ion to be substituted and the dopant, either electrons or holes appear in the *FeAs* layers. It is remarkable that there can occur a partial substitution for the atoms of the main layer, e.g., for Fe atoms with Co atoms; in this case, superconductivity is induced in the doped compound, in contrast to cuprates, where the substitution for Cu atoms located in the main layer destroys superconductivity.

1.4.1 Atomic Structure and Classification

Under ordinary conditions, zero-defect stoichiometric $LnOMPn$ (M = Mn, Fe, Co, Ni; Pn = P,As) phases have a layered tetragonal structure (*ZrCuSiAs* type, space

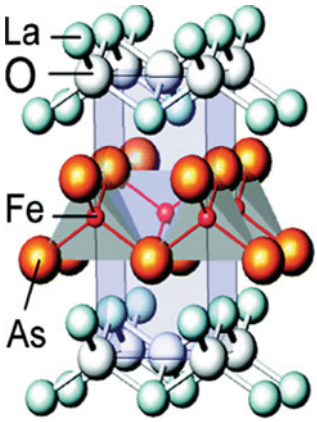

Fig. 1.13 Crystal structure of oxypnictide LaOFFeAs. The middle layer consists of Fe atoms (*red spheres*), which form a two-dimensional square lattice and As atoms (*yellow*). The second plane consists of O (*green*) and La (*gray*) atoms

group P4/nmm, $Z = 2$) [166] formed by stacking oppositely charged molecular layers $(LnO)/(MPn)$ along the $c-$axis (Fig. 1.13). It is immediately noted that for superconductors ($T_c > 26$ K) obtained on the basis of matrix 111-phase *LnOFeAs*; the electron concentration in $FeAs$ layers changes considerably pursuant as a result of the so-called modulation doping. For instance, the donor electrons in $FeAs$ layers can be due to a partial replacement of bivalent O_2^- anions by univalent F_1^- in neighboring LnO layers, which results in an increase in the difference between the charge states of LnO and $FeAs$ layers. Each MPn layer consists of a square net of M atoms, above and below which are the pnictogen Pn atoms. The transition metal atoms have coordination number (CNs) equal to four, and their coordination polyhedrons are MPn_4 tetrahedrons compressed along the c-axis. In other words, the MPn molecular layer can be represented as consisting of conjugate MPn_4 tetrahedrons. In turn, for the atoms of rare-earth elements Ln with CN $= 8$, the coordination polyhedrons CPs are distorted square LnO_4Pn_4 antiprisms; for oxygen atoms, CN $= 4$ and the CPs are OLn_4 tetrahedrons.

The crystal structure of tetragonal $LnOMPn$ is characterized by the lattice parameters $a(b = a)$ and c and by two so-called internal parameters z_{Ln} and z_{Pn}, respectively, determining the $Ln - O$ and $M - Pn$ interlayer spacings [166, 167]. The authors of [168] noticed a correlation between critical temperature and the $LnOFeAs$ lattice parameters: the T_c value decreases considerably with increasing the parameter a. This dependence is sometimes interpreted in terms of the internal or chemical pressure created by rare-earth metal atoms in the lattice, but the origin of such a correlation actually remains unclear. Another interesting correlation was found between T_c and the angles α_0 of $As - Fe - As$ bonds in $FeAs_4$ tetrahedrons that form $FeAs$ layers in the oxyarsenide structure. Critical temperature increases greatly as α_0 approaches $109,47^0$, i.e., when $FeAs_4$ groups assume a shape close to regular tetrahedrons. It was noted that such a structural transformation of $FeAs_4$ groups, for instance, in the structure of *NdOFeAs* was favored by oxygen vacancies in the composition of NdO layers [169].

The analogy between $FeAs$ systems and cuprates becomes even closer when we compare their crystal structures. FeAs systems are built of alternating FeAs planes separated by LaO planes, similar to how the alternating CuO_2 planes are separated by LaBa or YBa planes in cuprates. Systems of both types are strongly anisotropic because of their layered structure, and the electron states in them are quasi-two-dimensional. Soon after the REOFeAs compounds, compounds of the AFe_2As_2 type (A : Ba; Sr; Ca) were discovered, in which pairs of FeAs planes (bilayers), similar to the bilayers in cuprates of the $YBa_2Cu_3O_6$ type, alternate.

Thus, we now have three classes of compounds built from FeAs planes (LaOFeAs, AFe_2As_2, and LiFeAs) and analogous compounds of the FeSe type, in which superconductivity with relatively high T_c is revealed. Their physical properties are similar in many respects, which can be related to the similarity of their crystal structure, because in all cases it involves a common element, the FeAs layers. The highest values of T_c have been obtained in a number of doped REOFeAs compounds. At room temperature, all these compounds have a tetragonal structure belonging to the space group P4/nmm. Their crystal structure is formed by alternating $FeAs$ and LaO layers. An FeAs layer actually consists of three closely spaced atomic planes, which are arranged in a square lattice of Fe atoms, above and below, which there are located square lattices of As atoms arranged relative to the Fe plane such that each Fe atom is surrounded by a tetrahedron of As atoms. In other words, an FeAs layer is formed by $FeAs_4$ complexes. The spacing between $FeAs$ and LaO layers is $1.8A$. The crystal structure of LaOFeAs is shown in Fig. 1.13. It can be seen that the tetragonal unit cell has a rather elongated shape, which results in a strong anisotropy of all its properties and the quasi-two-dimensional nature of related electron states. The nearest neighbors of the Fe atoms are As atoms that separate the nearest adjacent Fe atoms, and hence the electron transfer over the iron sublattice is caused by FeAs hybridization; in this case, the exchange interaction between Fe atoms occurs not directly but through As atoms.

Typical results of measurements of anisotropy parameter of upper critical field H_{c2} on single crystals of 1111 [170] and 122 [171] systems are given in Fig. 1.14.

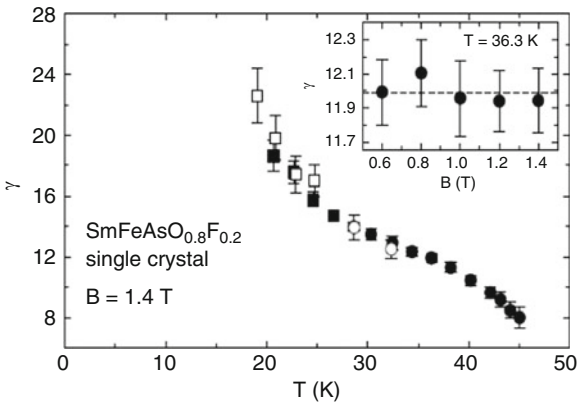

Fig. 1.14 Anisotropy parameter of upper critical field in Sm oxypnictide. Shown in the inset is the field dependence of the anisotropy parameter

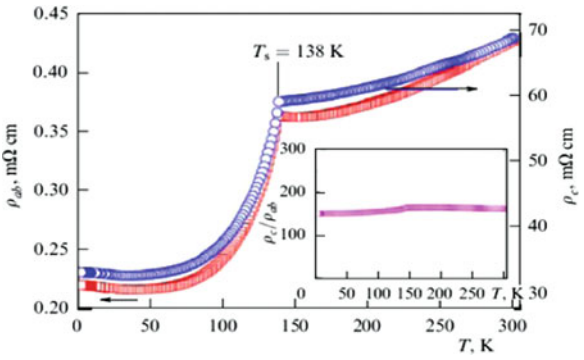

Fig. 1.15 Temperature dependences of resistivity r_{ab} in the ab plane and of transverse resistivity r_c in the orthogonal direction in a single crystal of $BaFe_2As_2$. Shown in the inset is the temperature dependence of the resistivity anisotropy

In particular, the anisotropy of the upper critical field H_{c2} testifies to the quasi-two-dimensional nature of the electronic subsystem in these superconductors, which is already evident from their crystal structure. At the same time, we can see that this anisotropy of critical fields is not too large. In Fig. 1.15, taken from [172] we depicted the temperature dependences of resistivity r_{ab} in the ab plane and of transverse resistivity r_c in the orthogonal direction for a single crystal of a prototype (undoped) $BaFe_2As_2$ system. It can be seen that the resistivity anisotropy exceeds 10^2, which confirms the quasi-two-dimensional nature of the electronic properties of this system. This anisotropy is significantly larger than the value, which can be expected from simple estimates based on the above-mentioned anisotropy of H_{c2}.

In the data given in Fig. 1.15, we can also clearly see an anomaly in the temperature dependence of resistivity at $T_s = 138$ K, which is connected with the antiferromagnetic transition. The question concerning the anisotropy of electronic properties has become more acute after measurements already evident from their crystal structure. In the study of anisotropy parameter of upper critical field H_{c2} in single crystals of $Ba_{1-x}K_xFe_2As_2$ [173] were performed in a much wider temperature interval than in [171], up to the field values on the order of 60T. According to [173], the anisotropy of H_{c2} is observed only in the relatively narrow temperature interval close to T_c, changing to almost isotropic behavior as the temperature lowers.

1.4.2 Electronic and Band Structure

First-principle calculations of the electronic structure of the LaOFeP compound, in which superconductivity ($T_c = 4K$) was revealed for the first time, were performed before the experimental detection of high T_c in this class of compounds [174]. The calculations for *LaOFeAs* were carried out almost simultaneously in a number of works [175–177]. The electronic structure of many *REOFeAs* compounds $RE = La; Ce; Sm; Nd; Pr; Y$ was also calculated in [178]. The energy band structure is shown in Fig. 1.14, which is borrowed from the earlier work [174] for the sole reason that the corresponding figure in [175] is complicated by additional data due to variations in the coordinates of *As* atoms in the lattice; at the same time, the calculations for *LaOFeP* in [174] are identical to those for *LaOFeAs*. As can be seen

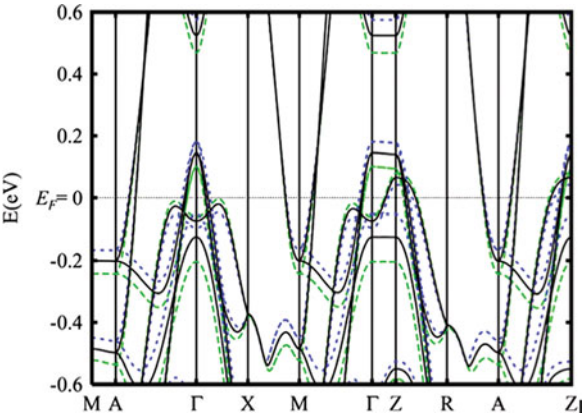

Fig. 1.16 Energy band structure of the LaOFeP compound. The unshifted band structure is indicated by the *solid black line*, while the shift away (towards) the Fe is indicated by the *blue dotted lines* (*green dashed lines*).The effect of As breathing along z taken into account. The symmetry points are $\Gamma = (0, 0; 0)$, $Z = (0, 0, 1/2)$, $X = (1/2, 0, 0)$, $R = (1/2, 0, 1/2)$, $M = (1/2, 1/2, 0)$, $A = (1/2, 1/2, 1/2)$

from Fig. 1.16, there are 12 dispersion curves. The Fermi level intersects two-hole bands, which proceed from the Γ point, and two electron bands, which proceed from the M point. We note the flatness of the curves in the direction ΓZ, which indicates a weak dependence of the hole quasiparticles on the momentum k_z; therefore, the Fermi surface in the vicinity of Γ has a cylindrical shape. The same relates to the Fermi surface sheets close to the M point (this follows from the flat segment of the curves on the line MA).

Thus, in the case of the $LaOFeP$ compound, two hole cylindrical sheets with their axes in the direction ΓZ and two electron sheets with axes along MA are formed on the Fermi surface. This indicates the quasi-two-dimensional nature of the electron states formed by the d_{xz} and d_{xy} orbitals. In addition to these four cylindrical sheets, there is a three-dimensional hole pocket centered at the Z point of the Brillouin zone (Fig. 1.17). This three-dimensional pocket is formed by d_z orbitals of Fe hybridized with p states of As and La. In oxypnictides in a narrow (0,2 eV) energy interval around the Fermi level, where the superconducting state is formed [179, 180]. It can be seen that electronic spectra of all systems in this energy interval are very close to each other. In the general case, the Fermi level is crossed by five bands formed by d-states of Fe. Of these, three form hole-like Fermi surface pockets close to the Γ point, and the others form two-electron-like pockets at the corners of the Brillouin zone (note that the Brillouin zones of 1111, 111, and 122 systems are slightly different due to existing differences in lattice symmetry).

It is not difficult to understand that this kind of a band structure leads to similar Fermi surfaces of these compounds presented in Fig. 1.17: there are three hole-like cylinders at the center of the Brillouin zone and two electron-like ones at the corners. The almost cylindrical form of the Fermi surfaces reflects the quasi-two-dimensional nature of the electronic spectra in oxypnictide superconductors.

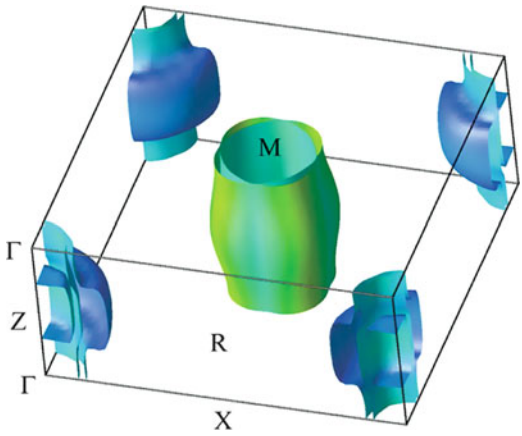

Fig. 1.17 Fermi surface of oxypnictide LaOFeAs: darker (*blue*) regions correspond to low velocity. The symmetry points are the same as in Fig. 1.16

The smallest of the hole-like cylinders is usually neglected in the analysis of superconducting pairings, as its contribution to electronic properties is rather small (the smallness of its phase space volume). At the same time, from the general picture of the electronic spectrum it is clear that superconductivity is formed in a multiple band system with several Fermi surfaces of different (electron or hole-like) natures, which is drastically different from the simple single-band situation in cuprate superconductors.

The study of the Fermi surface based on measurements of the de Haas-van Alphen effect, with quantum oscillations of magnetization in a magnetic field being was measured [181]. As the object of the study, the authors chose the compound $LaOFeP$ (of the same crystal structure as LaOFeAs), with the superconducting transition temperature $T_c = 7\,\mathrm{K}$. This choice was made because a single-crystal sample, first, of high purity and, second, with a low value of the upper critical field ($B_{c2} = 0,68T$ for the external magnetic field $B \parallel c$ and 7.2 T for $B \perp c$) was needed in order to suppress the superconducting state in experimentally accessible magnetic fields. The results obtained showed that this compound has two cylindrical hole surfaces centered at the Γ point and two electron surfaces centered at the M point, in complete agreement with the results of the LDA calculation in [174] but with higher effective masses (in the range 1,7–2.1m_e, where m_e is the mass of a free electron). The electron masses calculated for this compound are of the order of $0.8m_e$. Therefore, we have an experimental confirmation (obtained with the aid of different techniques) of the basic conclusions of LDA calculations for FeAs systems.

Thus, the main distinction of oxypnictide superconductors is their multiple band nature with anisotropy. An electronic structure in a narrow enough energy interval around the Fermi level is formed practically only from the d-states of Fe. The Fermi surface consists of several hole-like and electron-like cylinders and on each its "own" energy gap can be formed. Broadly speaking, this multiband character of superconductivity is not new and has already been analyzed in the scientific literature (see for details Chaps. 2 and 3). The specific band structure typical of FeAs layers, however, needs an additional analysis.

http://www.springer.com/978-3-642-22651-9

Unconventional Superconductors
Anisotropy and Multiband Effects
Askerzade, I.
2012, XIV, 178 p., Hardcover
ISBN: 978-3-642-22651-9